International Journal of Science and Research (IJSR)
ISSN: 2319-7064
SJIF (2020): 7.803

Automated Enhancement of Myocardium Images using Image Processing Methods

Yousif Mohamed Y. Abdallah[1,2,3*], Mohamed M.O Yousef[2,4], Eltayeb W. Eltayeb[1,2]

[1]College of Radiological Studies and Nuclear Medicine, National Rabit University, Khartoum, Sudan

[2]Sudan University of Science and Technology, College of Medical Radiological Science, Elbaladi Street, Khartoum 1908, Sudan

[3]Radiological Science and Medical Imaging Department, College of Applied Medical Science, Majmaah University, Majmaah, 11952, Saudi Arabia

[4] Diagnostic Radiology Department, Batterjee Medical College, Jeddah, Saudi Arabia
Corresponding author: *y.yousif[at]mu.edu.sa , yousifmohamed[at]sustech.edu*

Abstract: ***This was experimental study of 80 cardiac patients that conducted to Characterize of myocardial diseases using image processing technique. This study was performed in nuclear medicine department of Rabit Nation University in period of January 2016 to December 2020. In this thesis, the new medical image analysis methods were presented to characterize myocardial diseases using SPECT to differentiate between myocardial infarction and myocardial ischemia as well as the quantification of the normal heart tissues. There are many problems due to absence of SPECT imaging protocol which is very essential in diagnosis of cardiovascular disease and can be used to compare its effectiveness of other diagnostic modalities. The automatic delimitation technique was proposed of the SPECT cardiac images. The automated image enhancement, noise reduction and segmentation algorithms were used in this study to accurately delineate the myocardium structures compared with the other similar approaches. Automated methods of image processing, mainly of image registration, are integrated in a computational solution to automatically compute a set of features from myocardial perfusion SPECT images and use them to statistical analysis and classification of patient exams as from a healthy patient or with an associated disease. The image registration algorithms used, including the watershed-based segmentation, similarity measure, optimization, and interpolation algorithms, will be described and discussed, as well as the computational processing, analysis and classification techniques employed. The segmented images were projected onto the original images to demonstrate those projections and correlate them with the manual delineations. The experimental results of this study showed that the automated methods and visualization with high corresponding and matching rates.***

Keywords: Myocardium; Image processing, Heart; Nuclear medicine

1. Introduction

Radiotracers are frequently used to map the physiology and fluid streams of a tissue or organ because they aid in the diagnosis of physiological conditions in the body. In comparison to other imaging techniques such as computed tomography and nuclear imaging, which can produce images of structures that are not present, emission tomography modes simultaneously examine perfusion and metabolic activity [1]. Anesthesiologists, cardiologists, and psychiatrists use it to diagnose and confirm certain medical conditions. Along with improving image acquisition and analysis methods, critical areas of research include increasing the spatial and temporal resolution of digital medical images, which can be accomplished through higher resolutions. However, it should be noted that effective image analysis will not be possible until new or more integrated registration methods are developed [2-5]. Combining images acquired from multiple viewpoints, time acquisitions, and even subject atlases with a variety of medical imaging modalities such as positron emission tomography (PET), single photon computed tomography emissions (SPECT), computer tomography, and magnetic resonance imaging (MRI) enables the detection of anatomical differences (MRI). When used in conjunction with other techniques, SPECT can be used to assess both myocardial perfusion and ventricular function (GSPECT). Because image processing and quantification aided in the development of myocardial perfusion imaging's diagnostic and prognostic capabilities, image processing and quantification aided in the advancement of myocardial perfusion imaging's diagnostic and prognostic capabilities. Among the additional imaging techniques are the enhancement of perfusion data, the enhancement of overall information, the assessment of feasibility, and the sequential follow-up following therapy [5-8]. Nuclear medicine physicians must have a firm grip on visual interpretation in order to recognize and diagnose anomalies, as well as a firm grasp on border and criterion evaluation [9-15]. Myocardial infusion SPECT image interpretation likewise includes an atlas, but it covers the theoretical foundations in greater detail. Individuals with major blood circulation disorders have a more distinct endocardial shape, but their endocardial edge identification is erroneous 85. Individuals with smaller hearts may have imprecise measurements, whilst those with larger hearts will have more precise measurements. These studies used a combination of computer simulations and experiments [16-17]. Additionally, the left ventricular volume is depicted segmented with distinct cardiac zones inside each segment, as is the heart's LV ejection fraction (LVEF). New techniques are being used to determine left ventricular diastolic indices and mass 87. The patient's LV perfusion pattern is seen using a novel polar mapping technology, and

areas of hypoperfusion are identified using a second method. It is a technique for visualizing the maximum three-dimensional LV count distribution on a two-dimensional polar map. It is critical to observe that the polar intensity at the LV's base is on the periphery of the polar map, but the polar intensity at the LV's apex is within its heart [18-20]. The patient's cardiac 3D model's tracer accumulation ratio is compared to a lower statistically established normal limit for the left ventricle's volume or function that is less than the patient's cardiac 3D model's tracer accumulation ratio [21-22]. Calculating the degree of hypoperfusion is feasible using a blackout or polar map. Hypoperfused segments are identified and counted [23-24]. It is feasible. Due to the left ventricle's varied form, coronary artery mapping using computed tomography may be more accurate than standard computed tomography in determining left ventricle perfusion. Depending on the study, most heart perfusion studies report data in segments of 17 or 20 segments. The basal, middle, and apical thirds of the cardiac perfusion zone are split into three segments according to the 20-segment model: basal, middle, and apical thirds, with the apical cap divided into two segments. 30% of the foundation is built of the base; 30% of the foundation is composed of the intermediate capillary zone; 40% of the foundation is composed of the apex and apical cap. There is a correlation between coronary artery blood flow and the segmental distribution of the coronary arteries of the heart. The left anterior descending artery is divided into the following sections: one, second, third, seventh, eighth, and thirteenth; the right artery is divided into the following sections: four, nine, ten, six, and seventeen; and the right coronary artery is divided into the following sections: seventeen, twelve, six, six, and twelve. Individual variables such as data collection, data processing, quantification, and physiological variation all affect the reproducibility of results. For instance, complex data must be used to run these programs in order for them to be easily analyzed. To analyze and scrutinize the data, a subject matter expert (SME) with a strong professional background in statistics and visualization is required. Recently, in nuclear medicine has been extensively using imaging as a elementary means to assist in procedures' analyses, the progress of pathologies and preparation of treatments. Consequently, it becomes a basic method to help treatment choice through non-invasive procedures. Cardiac nuclear medicine is useful in diagnosing and assessing coronary artery diseases. It is also used to evaluate cardiomyopathy and identify possible damage to the heart from different disorders. The computational and Image Processing techniques allow the amalgamation of diverse medical image tools and the easier recognition of changes between scintographs acquired from diverse points of view, diverse acquisition times or even with subject atlas to attain prior anatomic or functional information. It stresses changes in size, shape, or image intensity over time, and relates both preoperative image and surgical plans to the physical reality of patients during intervention and aligns patient's anatomy to a standardized atlas. There are many problems due to the absence of the applications of computational techniques in SPECT imaging protocol, which is very essential in the diagnosis of cardiovascular diseases and can be used to compare its effectiveness with the subjective diagnostic method [25-26]. A solution that automatically computes and uses a series of features from SPECT myocardial perfusion images in order to conduct statistical analyses and classify images as belonging to or not belonging to subjects with myocardial infusion has been developed as a result of the integration of image recording and other computational techniques for medical image analysis. Researcher will go over the image registration algorithms that were used in detail, including the transformation, similarity measure, optimization, and interpolator algorithms, in addition to the segmentation and segmentation steps. When image classification methods are used in conjunction with the segmentation method's feature subset, the diagnostic performance of the system is significantly improved [27-28]. The steps involved in developing a computational solution can be divided into the following categories: The alignment of the slices under investigation in the gated myocardial perfusion SPECT images with the pre-built template image is called data registration. The statistical analysis and image classification are called image classification. Following that, each step, as well as the experimental results obtained at each stage, will be thoroughly explained. With this implementation, it is not intended to replace physicians' clinical judgment, but rather to assist them in clinical decision-making, for example, by supplementing cardiology medicine teaching [28-29].

2. Methods and Materials

2.1 Population of the study

The study population consisted of patients (18-68 years) presenting at nuclear medicine department in Elnieleen Medical center during the period from January 2016 to December 2020. All the data was collected for the nuclear examinations which were performed after patient preparation and all the procedure has been clarified to the patients before the scanning. The sample size consisted of 80 patients (160 SPECT images).

2.2 Data collection

A solution that automatically computes and uses a series of features from SPECT myocardial perfusion images in order to conduct statistical analyses and classify images as belonging to or not belonging to subjects with myocardial infusion has been developed as a result of the integration of image recording and other computational techniques for medical image analysis. Researcher will go over the image registration algorithms that were used in detail, including the transformation, similarity measure, optimization, and interpolator algorithms, in addition to the segmentation and segmentation steps. When image classification methods are used in conjunction with the segmentation method's feature subset, the diagnostic performance of the system is significantly improved. The steps involved in developing a computational solution can be divided into the following categories: The alignment of the slices under investigation in the gated myocardial perfusion SPECT images with the pre-built template image is called data registration. The statistical analysis and image classification are called image classification. Following that, each step, as well as the

experimental results obtained at each stage, will be thoroughly explained. With this implementation, it is not intended to replace physicians' clinical judgment, but rather to assist them in clinical decision-making, for example, by supplementing cardiology medicine teaching.

Ethical consideration

Special consideration was given to the right of confidentiality and anonymity of all participants. Anonymity was achieved by using the number for each patient to provide a link between the information collected and the patients. In addition, confidentiality was obtained by making the data collected accessible only to the researcher. Justice and human dignity have been viewed equally by teaching the selected patient an opportunity to participate in the research. The data was saved securely in passworded computer.

Machine used

All examinations were carried out with SPECT machine. On a notebook computer equipped with an Intel® Core i5-5200U CPU (4.0GHz) and 8 GB of RAM, this computation was carried out in MatLab (64-bit). Several image processing and classification technologies, including Matlab (2020b) and the Insight Toolkit (ITK) 4.3, were used to implement the image segmentation procedure.

Experimental work

A visualization of the heart in order for photos that must be identified to have a consistent collection of images to refer to, an image known as the SPECT image is developed. When developing something, it is possible to follow three distinct phases. Images of patients in good health, patients who are ill, and patients who are very ill are shown. people who are not feeling well are photographed. Each of the three steps begins with a segmented coronary artery map, and each of the three steps ends with another segmented coronary artery map. The template image contains the 12 slices that were used for each of the cardiac axes in the study. Four-dimensional template myocardial perfusion SPECT pictures are created from myocardial SPECT imaging data collected from healthy volunteers who have provided information about the location of their coronary arteries. The three-dimensional template image was selected based on the data from the dataset. It was then determined how the answers of the control group compared to the control image. The output of the recording technique was used to construct the template image. There is only one template image created in this instance. This process is illustrated in detail in Figure 1. If the patient is a girl or a male, then the heart's architecture will be different depending on the gender of the patient. Fixed pictures should be described using a cubic B-Spline interpolator, which allows the user to choose the origin, distance, direction, and size of the image by adjusting the parameters of the interpolator. It is necessary for the moving image to pass through in order to function effectively. An image intensity filter that rescales images is used to equalize the intensity of images. This is followed by the start of the registration process. Specifically, the phrase "split into two pieces" refers to two distinct pre-registration methods: one that is rigid and employs a pre-registration approach, and another that is deformable and employs the most effective pre-registration methodology for multi-resolution registrations. In this context, the phrase "split into two pieces" refers to the phrase "split into two pieces" refers to the phrase "split into two pieces."

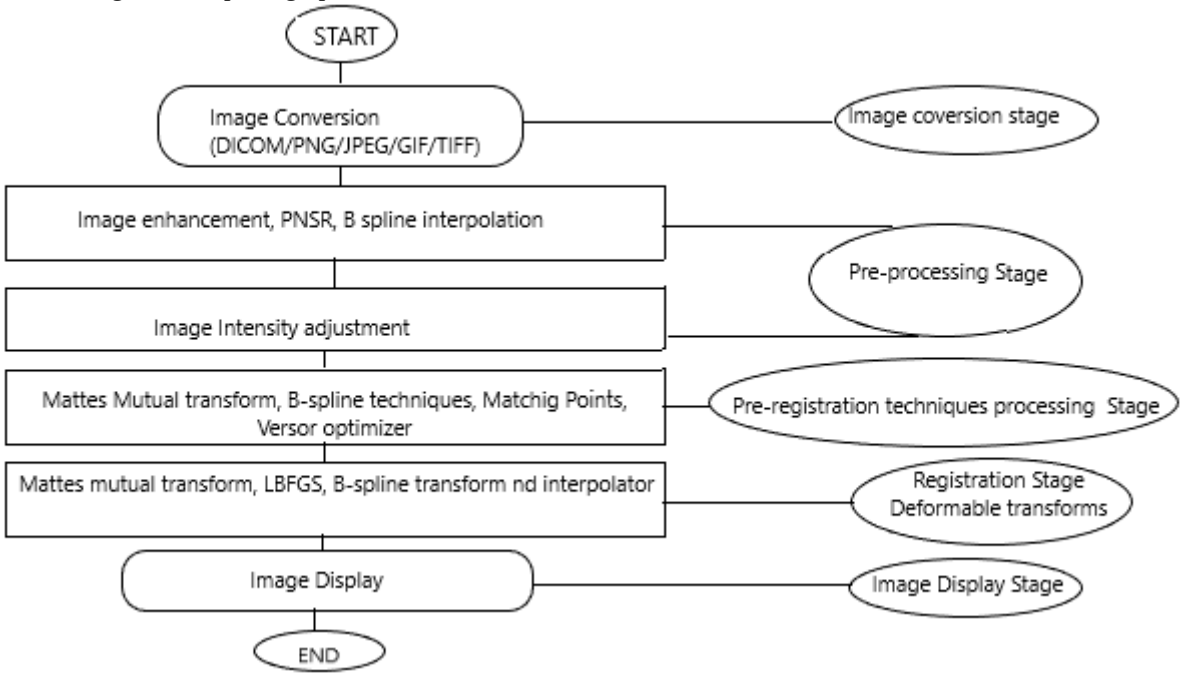

Figure 1: Image registration configuration and transforms

The pre-registration method is comprised of an initial translational pre-registration step and a final registration step. A centered transform initializer makes use of the center of mass determined by the image intensities of the input images as its starting point. An additional rigid 3D transform is then applied, which consists of three 3D rotations and three 3D translations, each specified by a versor and vector, respectively. The Mattes mutual information measure, which is based on information theory, is used to determine how much information one random variable can tell about

another random variable by using a single set of intensity samples to evaluate the marginal and joint probability density functions at discrete positions in the data set. The versor rigid 3D transform optimizer, which implements a gradient descent optimizer for the transformation parameter space, is the optimizer that searches for the best geometric transformation. The cubic B-Spline interpolator is the one that was used in this example. The most important parameters that must be defined in order to properly perform this pre-registration. This algorithm's values are presented in Table 2.2; these values were obtained experimentally, through trial and error, using the algorithm described. To register the pre-registered image with the reference image, following the acquisition of the pre-registered image, a final registration step based on deformable transformation must be performed. The left ventricular (LV) is segmented into two measurements. The first step is to extract and save DICOM volume slices in preparation for the second step. Because of the imaging system used, DICOM images have a low resolution. A new filter with a default pixel value of 10 is used to slightly increase the distance between the output and the camera. However, when the filter is applied to a template image with an output distance factor of 0.3, it produces a completely different outcome. The images are reprocessed to remove background noise after they have been rendered, and then morphological operations are performed on the images using median spatial filtering after they have been rendered. In order to create a base hat, an opening and closing technique was used after the initial creation of a top hat. When the slice containing the image is added, the lower hat is removed as a result. Increase the slice gradient of the SPECT image by performing this step. After performing K-means clustering on three clusters, the algorithm applies unsupervised learning to the three clusters in the dataset. In this location, the LV has already been divided. Filters for label maps are positioned around the object. Calculate the geometrical dimensions of the object, including its perimeter, spherical equivalent, roundness, elongation, and the number of pixels on the screen. It is necessary to create a geometric dimension in order to create a vector for each geometric dimension. There are five vectors that are generated as a result. Each vector contains a set of characteristics that were initially suggested for the target. This algorithm is illustrated in Figure 2.

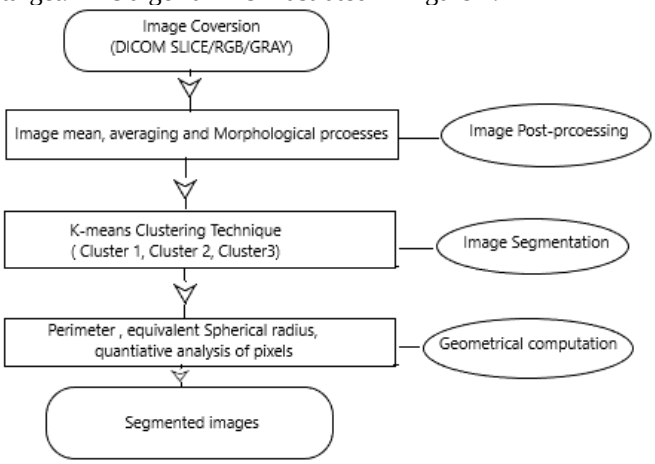

Figure 2: The Segmentation algorithm steps

The SPECT image of the coronary artery template of myocardial perfusion is currently complete. The two registration methods presented here are based on multi-resolution registration techniques and are fully described in the following sections. Because the registration algorithm was developed using previously obtained segmented images of two-dimensional objects, it could only be implemented in the two-dimensional domain. The algorithm, as well as the components for recording, are depicted in Figure 2. The pre-registration method makes use of the previously mentioned centralized transform initializer. Following that, the affinity is transformed from one line to the next, and so on. Mattes' mutual information is used to determine the similarity of two objects. Each descent algorithm is implemented using a standard descent optimizer. A linear interpolator is used to construct this set of characteristics. These values were discovered through a process of trial and error.

3. The Results

Early computer technology included the use of computational image registration techniques to build a SPECT myocardial perfusion template for use in SPECT myocardial perfusion imaging. The doctor double-checked the SPECT model photo to make sure that the registration procedure had been followed properly. Stress and relaxation segments are depicted in the SPECT pictures in Figures 3 and figure 4, respectively, using K-means clustering. It was necessary to align the coronary artery mapping with the template slices in order to generate picture slices for manual mapping. The results of the clinical stress protocol (as well as the results of the remaining assessments) are depicted in Figures. 5 and Figure 6.

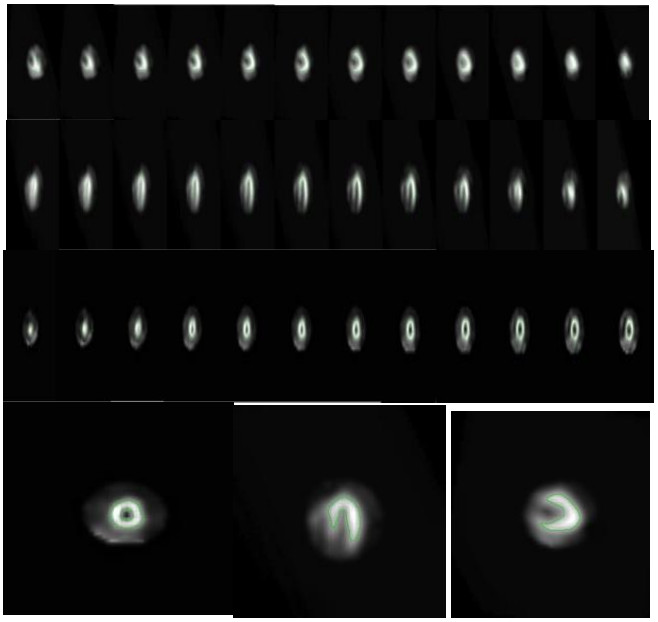

Figure 3: Segmented SPECT image obtained using registration techniques

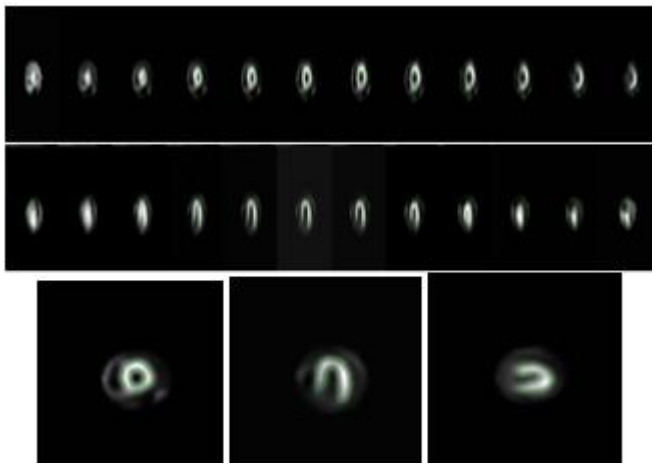

Figure 4: Segmented SPECT image obtained using registration techniques (Normal)

Figure 5: Twenty SPECT studies with coronary artery segments were conducted, and the results were published for stress studies: SA;HLA and VLA.

Figure 6: Twenty SPECT studies with coronary artery segments were conducted, and the results were published for rest studies: SA; HLA and VLA.

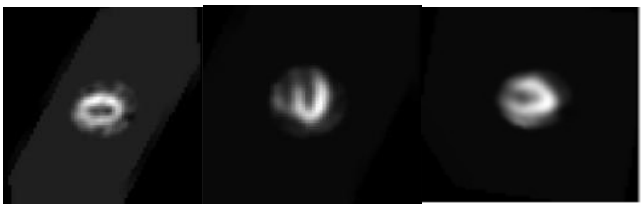

Figure 7: Twenty SPECT studies with coronary artery segments were conducted, and the results were published for rest studies.

Results of Application of K-means methods:

Figure 8: K-means transform (3 clusters).

1.1. Results of Region growing technique

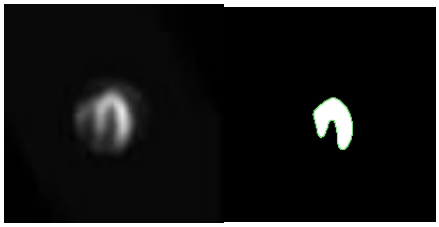

Figure 9: Region growing technique Segmentation

It is possible to calculate the effectiveness of a method. In the beginning, a 40-slice SPECT stress-myocardial image was segmented into 40 slices, and a gold standard was created by segmenting the image using the segmentation. For the first time, an approach was developed from scratch. This separation was made possible through the application of four independent processes, two of which were automatic in nature. Each accessible threshold is made up of three levels and three K-mean clusters, and there are many thresholds in each of these levels (see figure 3-9). In the MATLAB simulation results shown in Table 1, the estimated Dice coefficient can be seen as a percentage in the results of the simulation.

Table 1: Dice's coefficient computation between manual segmentation and five automated methods

Features	(Manual Score) ITKSNAP	Otsu	K-means Clustering	Region Growing	Shape Detection
Mean	0.604	0.768	0.783	0.747	0.819
Std. Dev.	0.092	0.059	0.057	0.038	0.057

The same slices used in the first half of this example were also segmented and reviewed manually by a clinical practitioner in the second section of this example. Table 2 is a summary of the outcomes of Dice's coefficients calculations.

Table 2: Dice's coefficient computation between a manual segmentation of a clinical expert and five automated methods

Features	(Manual Score) ITKSNAP	Otsu	K-means Clustering	Region Growing	Shape Detection
Mean	0.541	0.834	0.895	0.811	0.983
Std. Dev.	0.087	0.075	0.084	0.053	0.071

When determining the Dice coefficient, the k-means approach can be utilized to help. Following the application of k-means (3 clusters) to the myocardial SPECT segment template, useful myocardial infusion geometric metrics such as perimeter, spherical equivalent, roundness, elongation, and pixel count can be determined, which can be used to improve the accuracy of myocardial infusion imaging. Table 4.3 shows the mean values for each geometric dimension per axis for the stress and resting template images, as well as the mean values for the stress and resting template images.

Table 3: Geometric measurements of the segmented items

Procedure	Axis	Perimeter	Equivalent Spherical Radius	Roundness	Elongation	No. Pixels
Stress	SA	267.07 +55.7	29.23+ 7.4	0.80+ 0.04	1.14 + 0.4	643.8+74.8

	HLA	246.22+ 45.4	28.11+ 8.3	0.75+0.08	1.43+0.9	585.8+78.1
	VLA	286.45+ 60.1	34.09+ 9.2	0.82+0.05	1.26 + 0.7	902.27+104.6
Rest	SA	283.04+ 42.6	29.37+ 8.8	0.82+0.03	1.49 + 0.7	629.86+101.5
	HLA	309.81+ 52.4	40.04+ 7.9	0.79+0.02	1.71 + 0.9	806.52+99.8
	VLA	296.26+ 48.6	33.39+ 6.8	0.84+0.07	1.46 + 0.8	982.7+109.7

For evaluating the categorization technique, the terms "abnormality present" and "abnormality not present" are used interchangeably. According to the confusion matrix provided in Table 4, the values for healthy and sick individuals.

Table 4: Bayesian classifier results and Confusion matrix

Clinical decision	Algorithm judgment		
		Abnormality present	Abnormality not present
	Abnormality present	29	13
	Abnormality not present	9	53

As well as sensitivity and specificity, accuracy and a mean error rate were tested in addition to the five criteria. The findings were put through their paces. The parameters that were determined are listed in the preceding table, and the values that were obtained are listed in Table 5.

Table 5: Performance measures of the proposed classification technique.

Measure	Performance values
Sensitivity	0.745
Specificity	0.831
Precision	0.865
Accuracy	0.794
Mean error rate	0.132

4. Discussion

The results of this showed that 64 of them were male (62.14%) and 36 were female (37.86%). Using serial SPECT images, the researcher was able to create a template image and perform left ventricular segmentation on the core using the template image. Aims of this study were to determine whether a typical left ventricular infusion had a specific geometric dimension and, using statistical analysis, to determine whether or not patients had a cardiac issue. The attendees were separated into two groups for the purpose of discussion. Initially, rigid transforms are used to pre-register the model, which is followed by registration using deformable transforms and ultimately registration with rigid transforms. In order to correct global deformations before applying these sequential registration methods to localized deformations, they must first be applied to global deformations. Due to significant anatomical differences between male and female patients, it was challenging to identify components that consistently gave reliable data in both groups. Even when used in conjunction with other approaches, linear interpolators resulted in visually disturbing distortions when compared to the original data. Because of the curve fit and interactive curve design, the B-spline interpolator produced the best results while also being the most precise of the three interpolators. In spite of the fact that deformable registration methods are essentially based on data theory metrics, they are exceedingly flexible and adaptive to a broad variety of adjustments, and as such, they are employed in a huge number of stiff registration procedures. The algorithm will deal with the mutual information between Mattes and his friends. Visual confirmation was performed on both the SPECT coronary artery map template and the contemporaneous SPECT myocardial infusion template to ensure that they were correct. Because of the non-uniform image intensity, typical image processing techniques such as binary thresholding and gradient segmentation are unable to be used to cardiac-SECT data. As indicated in Table 2, table 3, clinical professionals produced the best results when they employed the Golden Standard and manual segmentation, as well as when they used K-mean clustering methods with three clusters and the dike coefficient. The approximate area is growing in both size and scope. However, in order to improve the accuracy of population segmentation, these variables must be more closely related to the dice coefficient than they currently are. These numbers are completely correct in every manner. A basic and successful segmentation strategy, as seen in this example, begins with picture enhancement, which is accomplished by advanced morphological and morphometric algorithms that decrease noise and clarify borders. Other data, such as lung and breast activity tracer retention, are unaffected and are consistent with a normal, non-hypertrophied right ventricle in the LV segment, as is the case in this case. According to the images in Figures 1-9, the left ventricle can be distinguished from the right ventricle in all of its sections. The boundaries of the division components have been delineated with great precision. Applying geometric and statistical factors related with categorization to the problem Table 3 displays the mean stress and residual images for each geometric dimension, as well as the overall stress values and residual images for the entire geometric dimension. In Table 3-5 are located just beneath the figures in the table. Table 35. In order to make the remaining measurements, the middle template's coronary artery mapping portion is segmented into numerous slices that have already been registered, thereby increasing the geometrical dimensions of each template, which are measured from the base to the apical of the coronary artery mapping portion. A single slice has been used as a reference for all sections as a result of this alignment. This has established a consistent link between the initial and final geometric dimensions of patient evaluation and the segmented structure geometric dimensions used by related classes, thereby altering classification outcomes. In accordance with the Bayesian classification, the system has a reasonable capacity for detecting abnormalities, with a detection rate of roughly 70 percent. Without an abnormality, the algorithm's false positive ratio, or its ability to declare a healthy test, is approximately 95%. The mean and standard deviation of the classification approach are lower when compared to the total number of healthy patients that completed the test using the test data package that was used. As a result of the decreased sample size of the test data

package that was employed, it is possible to justify the lower mean and standard differential values in classification. The accuracy and precision features of a system reveal that the system can accurately decide and detect in 83 percent and 88 percent of the cases, respectively. All aspects of the procedure, particularly the patient images and image template recording, which have been visually examined and are therefore more likely to be detected as having variability, should be tweaked to obtain an average error rate of 12.4%. When the situation becomes more serious small hearts have appropriate myocardial perfusion, while large hearts have insufficient myocardial perfusion. These are the most often encountered causes of the average error rate. It is possible that the geometrical dimension of the LV will change as a result of this adjustment, leading to erroneous reporting that could result in unwanted distortions. The classification system that was put in place was a success. The term "categorizing someone" refers to someone who categorizes other people. In order to overcome this issue, the photo registration technique described in this article has been refined and improved. In one clinical study, the average time required for each set of HLA, VLA, or SE photos for the calculation of patient and clinical protocol images was 8 minutes per set of photos (stress or rest). A possible explanation for this statistic is the restricted CPU power of the machine that was utilized to develop this computer solution.

5. Conclusion

Because there is no known SPECT image pattern in the scientific literature, one must be generated from scratch. At the time, it was decided to design a method based on deformable transformations in order to give myocardial SPECT imaging both during stress and at rest. A study was conducted to determine the quantity and location of cardiac anomalies in the patient's coronary arteries utilizing myocardial SPECT perfusion imaging, with the results manually identified and reported. Left Ventricle Nuclear Research Segmentation is a time-consuming and labor-intensive operation used to diagnose cardiac problems. It demands a great deal of patience and effort on the side of the patient. Automatic estimation of the deice coefficient is possible using the k-mean clustering technique described below (three clusters). Despite the range of topologies revealed by the findings, it is recommended that the dice coefficient be increased to near maximum values for all data sets comprising coronary artery mapping regions in order to obtain the best results. In comparison to other technologies, the constancy of this technique's functioning is crucial, as is its capacity to endure interference from low-resolution and noisy data. Despite the fact that men and women have a large variety of physical characteristics, the data suggest that the computational method may be capable of producing high-quality cardiac SPECT pictures for men and women with a wide variety of anatomical characteristics. It is feasible to easily address two key issues in the field of SPECT image processing by utilizing a single mathematical solution: noise and low-level features, which are explored more below. Due to the high specificity and accuracy of the classifier, it is necessary to improve image collection approaches in order to boost sensitivity while minimizing calculation time. This is critical in order to increase the classifier's sensitivity and error rate.

Conflict of interest statement

The authors declare that there is no conflict of interest regarding the main research, authorship, and publication of this paper.

References

[1] MUEHLLEHNER, Gerd; KARP, Joel S. Positron emission tomography. Physics in medicine and biology, 2006, 51.13: R117.
[2] JASZCZAK, Ronald Jack. The early years of single photon emission computed tomography (SPECT): an anthology of selected reminiscences. Physics in medicine and biology, 2006, 51.13: R99.
[3] PIMLOTT, Sally L.; SUTHERLAND, Andrew. Molecular tracers for the PET and SPECT imaging of disease. Chemical Society Reviews, 2011, 40.1: 149-162.
[4] MEYER, Jeffrey H.; ICHISE, Masanori. Modeling of receptor ligand data in PET and SPECT imaging: a review of major approaches. Journal of Neuroimaging, 2001, 11.1: 30-39.
[5] KHALIL, Magdy M., et al. Molecular SPECT imaging: an overview. International journal of molecular imaging, 2011, 2011.
[6] JASZCZAK, RONALD J.; COLEMAN, R. EDWARD. Single photon emission computed tomography (SPECT) principles and instrumentation. Investigative radiology, 1985, 20.9: 897-910.
[7] RAHMIM, Arman. PET vs. SPECT: in the context of ongoing developments. Iranian Journal of Nuclear Medicine, 2006, 14.1: 1-20.
[8] RAHMIM, Arman; ZAIDI, Habib. PET versus SPECT: strengths, limitations and challenges. Nuclear medicine communications, 2008, 29.3: 193-207.
[9] HUTTON, Brian F.; BUVAT, Irene; BEEKMAN, Freek J. Review and current status of SPECT scatter correction. Physics in medicine and biology, 2011, 56.14: R85.
[10] SPANOUDAKI, Virginia C.; ZIEGLER, Sibylle I. PET & SPECT Instrumentation. In: Molecular Imaging I. Springer Berlin Heidelberg, 2008. p. 53-74.
[11] DEPUEY, E. Gordon. Advances in SPECT camera software and hardware: currently available and new on the horizon. Journal of nuclear cardiology, 2012, 19.3: 551-581.
[12] PETERSON, Todd E.; FURENLID, Lars R. SPECT detectors: the Anger Camera and beyond. Physics in medicine and biology, 2011, 56.17: R145.
[13] BRANDERHORST, Woutjan, et al. Targeted multi-pinhole SPECT. European journal of nuclear medicine and molecular imaging, 2011, 38.3: 552-561.
[14] KHERUKA, S. C., et al. A study to improve the image quality in low-dose computed tomography (SPECT) using filtration. Indian journal of nuclear medicine: IJNM: the official journal of the Society of Nuclear Medicine, India, 2011, 26.1: 14.

[15] O'CONNOR, Michael K.; KEMP, Brad J. Single-photon emission computed tomography/computed tomography: basic instrumentation and innovations. In: Seminars in nuclear medicine. WB Saunders, 2006. p. 258-266.
[16] ROSENTHAL, M. S., et al. Quantitative SPECT imaging: a review and recommendations by the Focus Committee of the Society of Nuclear Medicine Computer and Instrumentation Council. Journal of nuclear medicine: official publication, Society of Nuclear Medicine, 1995, 36.8: 1489-1513.
[17] RITT, Philipp, et al. Absolute quantification in SPECT. European journal of nuclear medicine and molecular imaging, 2011, 38.1: 69-77.
[18] HINES, Horace, et al. National Electrical Manufacturers Association recommendations for implementing SPECT instrumentation quality control. Journal of Nuclear Medicine, 2000, 41.2: 383-389.
[19] VANDENBERGHE, Stefaan, et al. Iterative reconstruction algorithms in nuclear medicine. Computerized Medical Imaging and Graphics, 2001, 25.2: 105-111.
[20] ZANZONICO, Pat. Routine quality control of clinical nuclear medicine instrumentation: a brief review. Journal of Nuclear Medicine, 2008, 49.7: 1114-1131.
[21] SERET, Alain; FORTHOMME, Julien. Comparison of different types of commercial filtered backprojection and ordered-subset expectation maximization SPECT reconstruction software. Journal of nuclear medicine technology, 2009, 37.3: 179-187.
[22] Erwin, W. SPECT / CT Instrumentation and Clinical Applications. University of Texas, M. D. Aderson Cancer Center.2013.
[23] BOUCHARA, Frédéric; RAMDANI, Sofiane. Statistical behavior of edge detectors. Signal, Image and Video Processing, 2007, 1.3: 273-285.
[24] JACENE, Heather A., et al. Advantages of Hybrid SPECT/CT vs SPECT alone. Open Med Imag J, 2008, 13.2: 67-79.
[25] YANG, Feng, et al. Emerging inorganic nanomaterials for pancreatic cancer diagnosis and treatment. Cancer treatment reviews, 2012, 38.6: 566-579.
[26] DEFRISE, M. A short reader's guide to 3D tomographic reconstruction. Computerized Medical Imaging and Graphics, 2001, 25.2: 113-116.
[27] PFLUGER, Thomas, et al. Quantitative Comparison of Automatic and Interactive Methods for MRI–SPECT Image Registration of the Brain Based on 3-Dimensional Calculation of Error. Journal of Nuclear Medicine, 2000, 41.11: 1823-1829.
[28] STOKKING, Rik, et al. Normal fusion for three-dimensional integrated visualization of SPECT and magnetic resonance brain images. Journal of Nuclear Medicine, 1997, 38.4: 624-629.
[29] AZMAN, S., et al. A nuclear radiation detector system with integrated readout for SPECT/MR small animal imaging. In: Nuclear Science Symposium Conference Record, 2007. NSS'07. IEEE. IEEE, 2007. p. 2311-2317.

Author Profile

Yousif Mohamed Yousif Abdallah received the B.S., M.Sc. and PhD degrees and M.Sc. in nuclear medicine and Radiotherapy Technology from College of Medical radiological Science, Sudan University of Science and Technology in 2005, 2009 and 2013, 2014, respectively. During 2015 up to date, he is staying in college of applied medical Science, Majmaah University, Saudi Arabia. He is now associate professor of radiology.

Mohamed Mohamed Omer Yousef received the B.S., M.Sc. and PhD degrees and M.Sc. in Diagnostic radiology and nuclear medicine from College of Medical radiological Science, Sudan University of Science and Technology and National Rabit University, respectively. He is now associate professor of radiology in College of Medical radiological Science, Sudan University of Science and Technology. He is now associate professor of radiology and head of Diagnostic Radiology Department, Batterjee Medical College, Jeddah, Saudi Arabia.

Eltayeb Wagallah received the B.S. in nuclear medicine technology, Rabat University and M.Sc. and PhD in nuclear medicine from College of Medical radiological Science, Sudan University of Science and Technology in 2011 and 2014, respectively. During 2016 up to date, he is assistant professor of nuclear medicine. .